NANO LETTERS

2009
Vol. 9, No. 5
1999-2004

Facet-Dependent Electronic Properties of Hexagonal Silicon Nanowires under Progressive Hydroxylation and Surface Reconstruction

Xiaodan Xu and Peyman Servati*

Electrical and Computer Engineering, University of British Columbia, Vancouver, British Columbia V6T 1Z4, Canada

Received January 26, 2009; Revised Manuscript Received March 20, 2009

ABSTRACT

The effects of surface reconstruction and progressive hydroxylation on the electronic properties of [110] hexagonal silicon nanowires are investigated by ab initio calculations within the density functional theory. Progressive hydroxylation changes the density of states close to valence band maxima and leads to a general decrease in the band gap. The magnitude of band gap reduction is dependent on the facet where the hydroxyl group is bonded. While a high reduction in band gap (10%) is observed for hydroxylation on (111) facets, for (001) facets the reduction is more pronounced (21%) only when there is a (3 × 1) reconstruction. The reduction in band gap is generally accompanied by an off-center radial shift in the location of the charge density arising from the HOMO. These results go to show the impact of surface reconstruction and termination groups on the electronic properties of Si nanowires, which are important for using these materials for biosensor and transistor applications.

Silicon nanowires (SiNWs) have become promising for electronic applications such as transistors,[1] photovoltaic devices,[2] thermoelectric power generation, and biosensors[3] due to their unique properties such as large surface-to-volume ratio (SVR), high carrier transport mobility, and tunable band structure not present in the bulk. As quasi-one-dimensional material systems, SiNWs exhibit unique electronic and optical properties due to quantum confinement effects arising from their nanoscale cross section. For example, a direct gap is calculated for [110] NWs with hexagonal cross section with a diameter of up to 7 nm,[4] a phenomena that is promising for use of SiNWs in optoelectronic applications. While these properties are mainly determined by the diameter, crystallinity, and orientation of the NW core, they can be drastically influenced by surface properties including surface defects and surface termination bonds. Generally, the surfaces of Si NWs and nanocrystals are modified to control and reduce surface dangling bonds that can introduce electronic levels near the Fermi energy. For example, Tian et al.[2] have shown that the open circuit voltage and efficiency of SiNW photovoltaic devices can be enhanced by proper passivation of NW surface and grain boundaries due to suppression of recombination processes. In addition, dramatic improvements in carrier mobility, threshold voltage, and stability of poly-Si NW devices used in wet ambient conditions are primarily attributed to H^+ and/or OH^- surface passivation effects.[5]

Most of the theoretical calculations to date have been done to study the influences of crystalline orientations and the diameters on the electronic properties of SiNWs using ab initio density functional theory (DFT).[6−10] These DFT calculations have reliably predicted that as the diameter of silicon NWs and nanocrystals are reduced, quantum confinement leads to a general increase in the band gap. More specifically, the band gap of SiNWs is shown to linearly scale with SVR for different NW cross sections.[4] On the other hand, it has been shown that the interaction of the surface termination groups with the valence band edge competes against the quantum confinement effects and can induce a reduction in the band gap.[11] Recent theoretical studies on surface passivation focused on the effect of different types of chemicals and their surface coverage on electronic structure of SiNWs.[6,11,12] The effect of surface termination groups on electronic structure can change for different facets of SiNW, and the role of different facets in tuning the electronic properties is not clear yet. Recently, it was shown that bonding of radical NH_2 to the different facets can have different contributions to the density of states, which helps in choosing the right facets for making SiNW sensors.[13]

In this paper, we use state-of-the-art first principles calculations to investigate the effect of progressive hydroxylation on (111) and (001) SiNW facets and how the electronic

* Corresponding author, peymans@ece.ubc.ca.

10.1021/nl900271q CCC: $40.75
Published on Web 03/30/2009

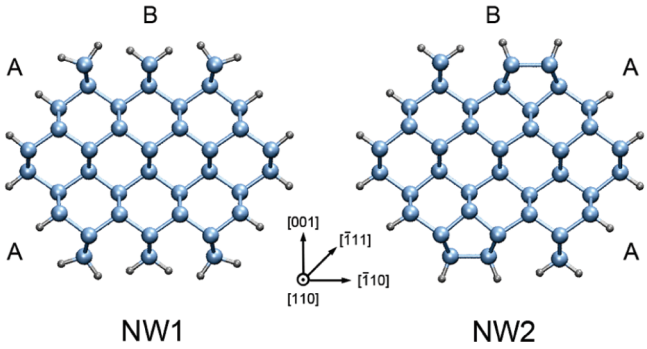

Figure 1. The cross section of the two types of SiNWs studied here after relaxation. The left structure is referred to as NW1 and the other NW2 with surface reconstruction as described in the text. NWs are oriented along [110]. Suffixes A and B denote (111)-type and (001)-type facets, respectively. The cyan balls represent Si atoms and the gray denotes H atoms.

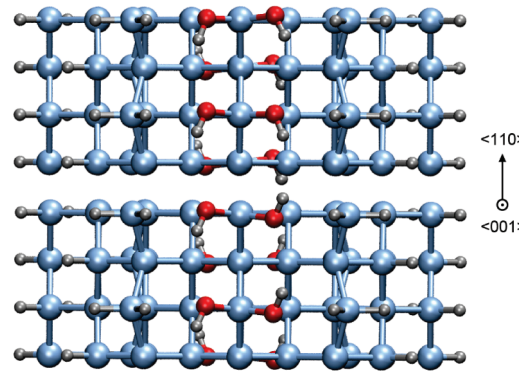

Figure 2. Cis (top) and trans structures (bottom) of hydroxyl groups on the (001) facets of NW1B-4OH after structural relaxation. The cyan, red, and gray balls represent the Si, O, and H atoms, respectively.

properties are affected by the facet morphologies. Hydroxyl groups on the surface are important models for technologically relevant processes including oxidized SiNW surfaces and can be used to prepare an ideal surface for atomic layer deposition of metal oxide dielectrics, based on ligand exchange reaction. Many theoretical studies on hydroxylation of silicon nanocrystals have been reported in the past years.[14,15] Here, we consider small diameter [110] SiNWs that are shown to be preferred due to development of lower energy surfaces such as (111) and (001). We also explore surface reconstruction in (001) planes. The sensitivity of different facets to hydroxylation is shown to be dependent on the presence of surface reconstruction.

The SiNW structures have been constructed along the [110] direction with hexagonal cross section and diameters of about 1.7 nm which have been observed experimentally.[16,17] Reference 18 has predicted that hexagonal wires become stable starting at about 1.2 nm diameter which is close to a recent reported experimental value of about 3 nm.[18] Each nanowire contains four (111)-type facets and two (001)-type facets which are the low-free-energy planes for ξ growth axis.[16] On the (111)-type facets, each Si atom is bonded to a single H atom. For the (001) facets, two surface structures were considered in order to study the effects of (001) surface reconstruction. The first type is the symmetric SiH_2 dihydrides structure (labeled NW1) where two H atoms are bonded to one Si atom (Figure 1). The other type (denoted as NW2) involves surface reconstruction (Figure 1) on the (001) facets where a pair of H atoms on each (001) facet are removed and an additional Si−Si bond is formed. This modification is referred to as a (2×1) surface reconstruction which is well studied for bulk Si(001) surfaces. Since there is one dihydride left on each (001) facet, the reconstructed (001) surfaces become a (3×1) structure which has been observed for bulk silicon (001) surface by scanning tunneling microscopy (STM).[19,20] For both surface structures, we first study the NW with full H-passivation, followed by gradual introduction of hydroxyl (−OH) on (001) or (111) facets. We use suffix A to denote OH-passivation on (111)-type facets and use suffix B for OH passivation on (001)-type facets. For example, NW2A-4OH is the NW with surface reconstruction where four H bonds on (111) facets of one unit cell are replaced by OH. The calculations in this work have been performed in the framework of ab initio DFT[21] within the local density approximation (LDA).[22] We have used a double-ζ polarized basis[23] set with pseudopotential constructed using a Troullier−Martins scheme.[24] The structural relaxation was performed using conjugated gradient minimization such that the force on each atom is less than 0.04 eV/Å. The distance between the NW and its images was about 18 Å, which is enough to avoid any interactions between the NW images. The cutoff for the grid integration was taken to be 200 eV. The Brillouin zone was sampled by up to five Monkhorst−Pack k-points along the nanowire axis. To calculate the electronic density of states (DOS), the Brillouin zone sampling was increased to 11 k-points.

Figure 1 shows a schematic of SiNW after relaxation, demonstrating a bulklike configuration due to the H-passivation layer. Due to the strong interaction between the adjacent dihydrides on the (001) facets of the NW1 category, the dihydrides repel each other and slightly rotate toward the (111) facets in the relaxed structure as shown in Figure 1. In the relaxed structure of NW2, the single dihydride on (001) facet does not rotate because of the (3×1) reconstruction on the surface. We also found that the O−H bonds on the (001) facets will be different from that on the (111) facets. Figure 2 shows two hydroxyl groups bonding to a single Si atom on the (001) facet of NW1B-4OH. Both cis and trans structures can be observed on the (001) facets with no reconstruction, while the hydroxyl groups on the (111) facets are symmetric and located in the cross-section plane of the NW. In contrast, in the NW2 category because of the larger H−H separation on the (001) facets, hydroxyl groups are in the same cross-sectional plane of the NW.

The formation energy of the NW system can be calculated by[7]

$$E_{\text{form}} = E_{\text{tot}}(\text{wire}) - \sum_{i=\text{Si,O,H}} N_i \mu_i \qquad (1)$$

where E_{tot} is the total energy of the nanowire, i represents different species, and μ_i is the corresponding chemical

Table 1. Calculated Total Energies, Electronic Band Gap (E_g) for All Systems[a]

system	E_{form} (eV)	CB (eV)	VB (eV)	ΔE_g (%)
NW1	5.512	−3.819	−5.142	
NW1A-2OH	−25.038	−3.827	−5.094	−4.23
NW1A-4OH	−55.578	−3.870	−5.064	−9.76
NW1B-2OH	−25.447	−3.809	−5.101	−2.37
NW1B-4OH	−57.708	−3.807	−5.077	−4.15
NW2	4.834	−3.856	−5.156	
NW2A-2OH	−25.732	−3.878	−5.113	−5.03
NW2A-4OH	−56.356	−3.955	−5.104	−11.58
NW2B-2OH	−25.866	−3.983	−5.105	−13.69
NW2B-4OH	−57.436	−3.788	−4.813	−21.18

[a] ΔE_g (in percentage) is the change in the energy gap compared to the original systems (NW1 or NW2) with full hydrogen passivation.

potential of the species. The chemical potential of silicon is taken as that of bulk silicon, and the chemical potential of hydrogen and oxygen are extracted from molecular hydrogen and oxygen, respectively. The formation energy analysis (see Table 1) shows that the H-passivated NWs are metastable as indicated by their positive formation energies.[25] The surface-reconstructed structure (NW2) is more stable than NW1 with an energy difference of 0.678 eV due to a larger separation of hydrogen atoms on the surfaces. We can also see that both NW structures show a monotonically decreasing formation energy as the number of OH radicals increase, implying that hydroxylation is an energetically favorable process. Interestingly, we found that for the same number of OH groups, hydroxylation on (001)-type facets results in lower energy than that on (111)-type facets. This can be clearly observed from the formation energies of NW1A-4OH and NW1B-4OH. This is also the case for surface-reconstructed NW that shows hydroxylation on (001)-type facets is more energetically stable (see NW2B-4OH and NW2A-4OH).

In this report, a direct band gap is seen (Figure 3) in all calculations, as the valence band peak and the minimum of the conduction band are at the Γ points. The band gaps we obtained for NW1 (1.3231 eV) and NW2 (1.3002 eV) are similar to the results of the hydrogenated SiNWs reported in ref 9. The lowest band gap is found in NW2B-4OH which is 1.0248 eV. As discussed in ref 11, although LDA-DFT calculations underestimate the band gap of [110] nanowires, the trends in the band gap can still be predicted correctly.[26,27] Comparing the band gap of the NW1 group and that of the NW2 group, we can see that (001) surface reconstruction induces a red shift in the band gap, which has been observed experimentally in silicon nanoparticles.[15,28,29] However, ref 12 showed that (001) surface reconstruction leads to a larger band gap due to the slight reduction in effective size. To further investigate the surface reconstruction effect on the band gap, we calculated the change in band gap for two SiNWs with hexagonal cross section but different diameters and surface-to-volume ratios. As shown in Table 2, for the SiNW with diameter about 2.6 nm, the change in the band gap due to surface reconstruction is 2.36% larger. In contrast, for the SiNW with diameter of about 1.4 nm (i.e., smaller than our current NW), a stronger red shift is observed: the band gap is reduced to 3.27 eV after surface reconstruction. On the basis of these results, we conclude that the impact of surface reconstruction on the band gap is size-dependent, which explains the discrepancy with ref 12.

Generally, hydroxylation reduces the energy gap in comparison to H-passivation. As shown in Figure 3, the change in the maximum energy of valence band is more significant as compared to the change in the minimum of the conduction band. For NW1A-2OH, NW1A-4OH, and NW2, the second valence band maximum is located just below the first one. Comparing NW1, NW1A-2OH, and NW1A-4OH, it can be observed that the reduction in the band gap values becomes more effective as the surface coverage of OH increases. The band gap of NW1A-2OH is reduced by 4.23%, while for NW1A-4OH it is reduced by 9.76%. However, the effect of OH passivation on (001)-type facets is different from that on (111)-type facets. Since NW1A-4OH and NW1B-4OH have the same number of atoms, we can compare them directly with NW1. The energy gap is only reduced by 4.15% with four OH bonded on the (001) facets, while the passivation on (111) facets with the same amount of OH shrinks the energy gap by 9.76%, which is more than twice larger. In contrast, the same analysis on NW2 shows that the reconstructed (001) facets seem to be more active in band gap modification. The band gap of NW2B-4OH is reduced by 21.18% with respect to NW2. These results go to show that the effect of hydroxylation is strongly facet dependent, which is very important for design and implementation of NW based biological and chemical sensors due to the fact that the density of carriers in NWs changes exponentially with a change in the band gap.

Table 3 summarizes the corresponding effective masses for different NWs. The effective masses of holes and electrons are determined directly from the curvatures of the valence and the conduction bands, respectively. The calculated effective masses of NW1 and NW2 which are passivated only with hydrogen agree well with the results reported in ref 30. As expected, the changes in electronic band structure lead to changes in the effective masses. It is found that for both NW1 and NW2 groups the effective mass of electron increases slightly as OH is introduced to the (111)-type facets (NW1A and NW2A in Table 3). In contrast, hydroxylation on (001) facets decreases effective masses for both electrons and holes. However, this trend in the change of effective masses is not observed in the SiNWs with surface reconstruction (NW2 category in Table 3). Our results show that the effective masses of electrons in NW2 category are generally smaller than that of NW1, while the effective masses of holes are larger as compared to the NW1 group.

After the structures were fully relaxed by the DFT-LDA approach, the molecular orbitals were calculated at the B3LYP/6-31G(d)[31] level of theory using the Gaussian 03 package.[32] It is found that the presence of hydroxyl groups on the NW surfaces delocalizes the highest occupied molecular orbitals (HOMO), while the lowest unoccupied molecular orbitals (LUMO) remain highly localized at the center of the NW (not shown here). Figure 4 shows the HOMO of NW1 and NW2 with and without hydroxylation. The charge distributions are generally around the Si−Si bonds along the nanowire's axis. When the NW is fully

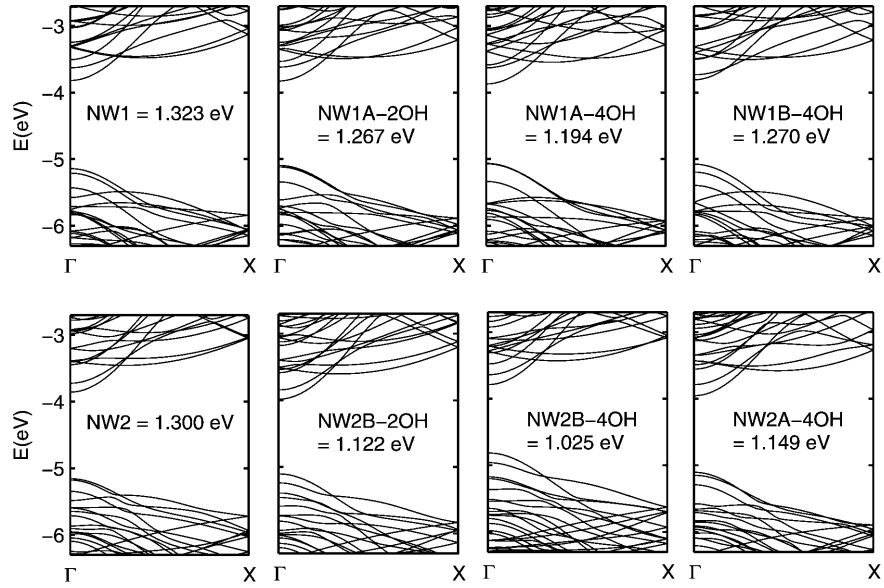

Figure 3. Electronic band structures and band gap of different SiNWs. The Fermi levels are all in the middle of the band gaps. k-points are sampled along Γ−X.

Table 2. The Changes in the Electronic Band Gap Due to (001) Surface Reconstruction for NWs with Different Diameters[a]

D (nm)	E_g (eV)	E_g' (eV)	ΔE_g (%)
1.4	1.402	1.356	−3.28
1.7[b]	1.323	1.300	−1.74
2.6	1.102	1.128	2.36

[a] ΔE_g (in percentage) is the change in the energy gap compared to the structure before surface reconstruction. [b] The NW with diameter 1.7 nm corresponds to NW1 shown in Figure 1.

Table 3. Calculated Ratios of Effective Masses for Electron (m_e*) and Hole (m_h*) to the Mass of a Free Electron (m) for All Systems

system	m_e*/m	m_h*/m
NW1	0.1260	0.1614
NW1A-2OH	0.1265	0.1649
NW1A-4OH	0.1270	0.1656
NW1B-2OH	0.1244	0.1584
NW1B-4OH	0.1247	0.1545
NW2	0.1191	0.1785
NW2A-2OH	0.1194	0.1703
NW2A-4OH	0.1203	0.1560
NW2B-2OH	0.1186	0.1613
NW2B-4OH	0.1197	0.1634

passivated with hydrogen, the HOMO is concentrated more in the interior of the NW. As OH passivation increases on the (111)-type facets of both types of NWs, the HOMO densities spread out to the surface and mostly toward the hydroxyl groups. However, hydroxylation on the (001) facets shows different results for NW1 and NW2. While for NW1 hydroxylation does not change the HOMO significantly, for NW2 the hydroxyl groups displace the HOMO states toward the surface. In NW1B-4OH, a large contribution around the center of NW remains and the induced surface states are small. Note that the nonsymmetric nature of HOMO densities for NW1B-4OH is due to the cis and trans structures on two (001) facets. In NW2B-2OH/4OH, although the interior orbital remains, there is a significant contribution from the passivation sites as well on the reconstructed surfaces. The difference must be due to the different surface structure of the (001) facets. We can conclude that the common effect observed in both NW1 and NW2 categories due to surface modification is that hydroxylation on (001) facets does not change the HOMO around the center of the wire, while OH-passivation on (111) facets can significantly shift the HOMO from the center to a close proximity of the passivation sites. This can explain the change in the electronic band structures. The surface states induced by OH passivation cause significant changes in the valence band maxima (VBM) at the Γ point, while the conduction band minima (CBM) are relatively stable.

In order to understand the effect of hydroxylation on the electronic band structures, we also examine the partial density of states (PDOS). The total electronic DOS was decomposed into partial atomic contributions from different species and atoms at different sites. The PDOS curves were normalized by the total number of atoms. A Gaussian broadening of 0.05 eV was used. The PDOS contributions form the terminating groups (H, O) and the two types of Si atoms (one on the surfaces and one around the center) of NW1A-4OH are displayed in Figure 5. As reported in ref 13, the surface states of SiNWs seem to be more relevant in the formation of the VBM states. The main contribution to the DOS near the VBM is from the Si atoms at the hydroxyl sites (in this case on (111) facets), as can be seen in Figure 5 by comparing the first peaks of the PDOS graphs of different atoms. The next two contributions, although at lower level, are from the O atom at the hydroxyl site and the Si atom around the center. However, the contributions from the Si atom on the facets with no hydroxyl group (i.e., (001) facets in this case) and the H atoms are relatively small. Similar effects are observed in NW2A-4OH and NW2B-4OH as well.

Since we know Si atoms play an important role in the DOS, we then plot the PDOS derived from Si atoms at different sites for both NW1 and NW2 categories. The three

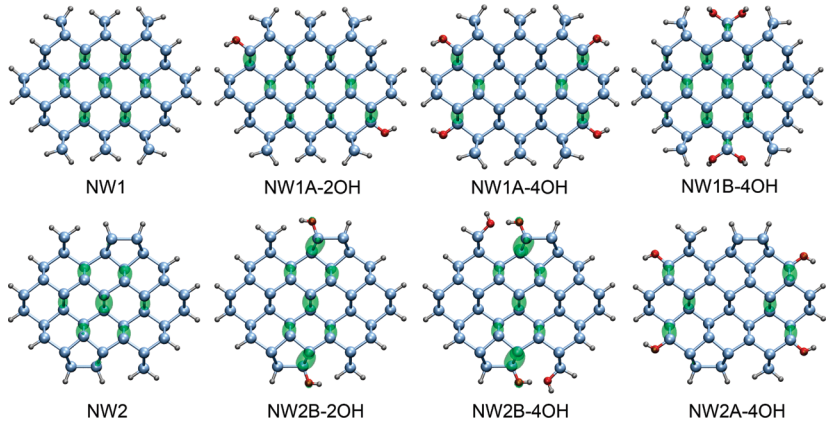

Figure 4. HOMO orbitals (of the same contour value 0.045) associated with different NW systems. The cyan, red, and gray balls represent the Si, O, and H atoms, respectively.

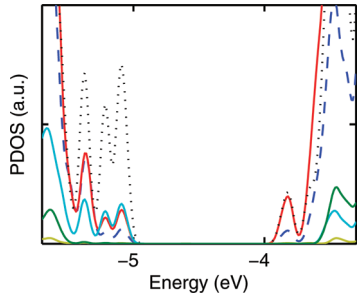

Figure 5. PDOS plots for H (yellow solid), O (cyan solid), and Si (black dot) atoms on (111) facets, H (green solid) and Si (blue dash) atoms on (001) facets, and Si (red solid) atoms around the center for NW1A-4OH.

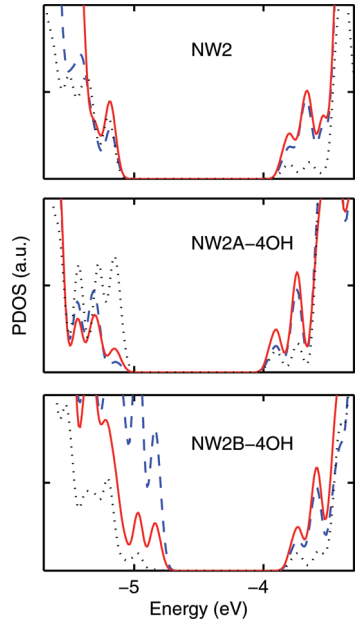

Figure 6. PDOS of silicon atoms on (001) surface facets (blue dash), (111) surface facets (black dot), and around the center (red solid) for NW2, NW2B-4OH, and NW2A-4OH.

plots in Figure 6 are for NW2, NW2B-4OH, and NW2A-4OH, respectively. For NW2 with H only passivation, the contributions of the silicon atoms on (001) and (111) facets and around the wire center to the DOS near the valence band edges are very similar. For NW2B-4OH where hydroxyls

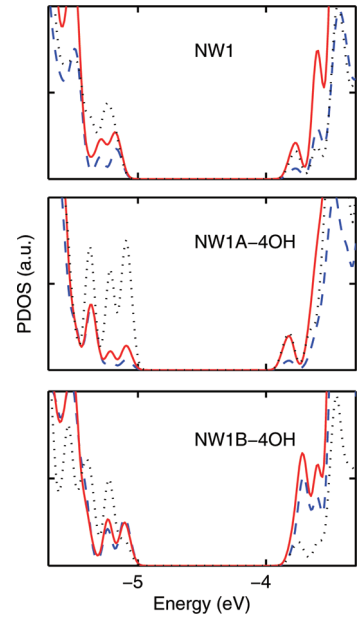

Figure 7. PDOS plots of silicon atoms on (001) surface facets (blue dash), (111) surface facets (black dot), and around the center (red solid) for NW1, NW1A-4OH, and NW1B-4OH.

are absorbed on the (001)-type facets, the contribution to the valence band edge from the Si atoms on (111) facets dominates which is about 3 times larger. When hydroxyls are absorbed on the (111)-type facets (NW2A-4OH), the Si atoms on (111) facets contribute the most. This is consistent with the fact that the HOMO densities move toward the hydroxyl sites. For the states near the CBM, the contribution from the central atoms always dominates. But there is no significant difference among the Si atoms from these three sites. Figure 7 shows similar PDOS analysis for NWs from NW1 group. In contrast to NW2 group, where both the reconstructed (001) and the monohydrated (111) facets have significant contributions to the band-edge, the monohydrated (111) facets of NW1 seems to be more active than the symmetric (001) facets. Hydroxylation on the symmetric (001) facets of NW1 does not create states close to VBM. This difference must be due to the variation in the (001) facet morphology as observed in the HOMO density.

In conclusion, we have investigated the effect of hydroxylation and surface reconstruction on electronic properties of SiNWs including band gap, effective mass, and density of states. In contrast to confinement effects, the size of the band gap decreases by increasing the amount of hydroxyl groups on the surface. The decrease in band gap is more pronounced (∼10%) for hydroxyl groups on (111) facets in comparison to those on (001) facets (∼4%), when there is no reconstruction. But for NWs with reconstructed (001) facets, the decrease in band gap of about 21% can be observed for hydroxylation on reconstructed surfaces. The decrease in band gap of these NWs is accompanied by a general movement of charge densities arising from HOMO from the center of NW toward the surface. While effective masses for electrons and holes do not significantly change upon hydroxylation, reconstruction induces a small decrease in effective mass of electrons and a small increase in effective mass of holes. PDOS analysis for hydroxylated NWs also shows that the contributions of the surface Si atoms on either (001) or (111) facets will dominate the density of states around the VBM. The sensitivity of density of states to hydroxylation on (111) facets is pronounced for NWs with no surface reconstruction, while this is more pronounced for hydroxylation on reconstructed (001) surfaces. These results are important for understanding the effect of surface termination on the electronic properties of SiNWs and can be used for design of NW sensors and optimization of surface chemistry for SiNW transistors.

Acknowledgment. We gratefully acknowledge the financial support of the Natural Sciences and Engineering Research Council (NSERC) of Canada for this project. We also thank Dr. Alireza Nojeh for helpful discussions.

References

(1) Cui, Y.; Zhong, Z.; Wang, D.; Wang, W. U.; Lieber, C. M. *Nano Lett.* **2003**, *3*, 149. Colli, A.; Fasoli, A.; Beecher, P.; Servati, P.; Pisana, S.; Fu, Y.; Flewitt, A. J.; Milne, W. I.; Robertson, J.; Ducati, C.; De Franceschi, S.; Hofmann, S.; Ferrari, A. C. *J. Appl. Phys.* **2007**, *102*, 034302.
(2) Tian, B.; Zheng, X.; Kempa, T. J.; Fang, Y.; Yu, N.; Yu, G.; Huang, J.; Lieber, C. M. *Nature (London)* **2007**, *449*, 885.
(3) Lin, M. C.; Chu, C. J.; Tsai, L. C.; Lin, H. Y.; Wu, C. S.; Wu, T. P.; Wu, Y. N.; Shieh, D. B.; Su, Y. W.; Chen, C. D. *Nano Lett.* **2007**, *7*, 3656.
(4) Yao, D.; Zhang, G.; Li, B. *Nano Lett.* **2008**, *8*, 4557.
(5) Lin, H. C.; Su, C. J.; Hsiao, C. Y.; Yang, Y. S.; Huang, T. Y. *Appl. Phys. Lett.* **2007**, *91*, 202113.
(6) Ng, M. F.; Zhou, L.; Yang, S. W.; Sim, L. Y.; Tan, V. B. C.; Wu, P. *Phys. Rev. B* **2007**, *76*, 155435.
(7) Aradi, B.; Ramos, L. E.; Deak, P.; Köhler, Th.; Bechstedt, F.; Zhang, R. Q.; Frauenheim, Th. *Phys. Rev. B* **2007**, *76*, 035305.
(8) Vo, T.; Williamson, A. J.; Galli, G. *Phys. Rev. B* **2006**, *74*, 045116.
(9) Singh, A. K.; Kumar, V.; Note, R; Kawazoe, Y. *Nano Lett.* **2006**, *6*, 920.
(10) Zhang, R. Q.; Lifshitz, Y.; Ma, D. D. D.; Zhao, Y. L.; Frauenheim, T.; Lee, S. T.; Tong, S. T. *J. Chem. Phys.* **2005**, *123*144703.
(11) Nolan, M.; O'Callaghan, S.; Fagas, G.; Greer, G.; Frauenheim, T. *Nano Lett.* **2007**, *7*, 34.
(12) Leu, P. W.; Shan, B.; Cho, K. *Phys. Rev. B* **2006**, *73*, 195320.
(13) Leao, C. R.; Fazzio, A.; da Silva, A. J. R.; et al. *Nano Lett.* **2007**, *7*, 1172.
(14) Carniato, S.; Gallet, J. J.; Rochet, F.; Dufour, G.; Bournel, F.; Rangan, S.; Verdini, A.; Floreano, L. *Phys. Rev. B* **2007**, *76*, 085321.
(15) Ramos, L. E.; Furthmuller, J.; Bechstedt, F. *Phys. Rev. B* **2004**, *70*, 033311.
(16) Wu, Y.; Cui, Y.; Huynh, L.; Barrelet, C. J.; Bell, C. D.; Liber, C. M. *Nano Lett.* **2004**, *4*, 433.
(17) Ma, D. D. D.; Lee, C. S.; Au, F. C. K.; Tong, S. Y.; Lee, S. T. *Science* **2003**, *299*, 1874.
(18) Chan, T. L.; Ciobanu, C. V.; Chuang, F. C.; Lu, N.; Wang, C. Z.; Ho, K. M. *Nano Lett.* **2006**, *6*, 277.
(19) Boland, J. J. *Phys. Rev. Lett.* **1990**, *65*, 3325.
(20) Boland, J. J. *Surf. Sci.* **1992**, *261*, 17.
(21) Ordejon, P.; Artacho, E.; Soler, J. M. *Phys. Rev. B* **1996**, *53*, R10441.
(22) Zhao, X.; Wei, C. M.; Yang, L.; Chou, M. Y. *Phys. Rev. Lett.* **2004**, *92*, 236805.
(23) Sankey, O. F.; Niklewski, D. J. *Phys. Rev. B* **1989**, *40*, 3979.
(24) Troullier, N.; Martins, J. L. *Phys. Rev. B* **1991**, *43*, 1993.
(25) Ponomareva, I.; Menon, M.; Srivastava, D.; Andriotis, A. N. *Phys. Rev. Lett.* **2005**, *95*, 265502.
(26) Puzder, A.; Williamson, A. J.; Gro ssman, J. C.; Galli, G. *Phys. Rev. Lett.* **2002**, *88*, 097401.
(27) Puzder, A.; Williamson, A. J.; Gro ssman, J. C.; Galli, G. *J. Chem. Phys.* **2002**, *117*, 6721.
(28) Vasiliev, I.; Martin, R. M. *Phys. Status Solidi B* **2002**, *233*, 5.
(29) Puzder, A.; Williamson, A. J.; Reboredo, F. A.; Galli, G. *Phys. Rev. Lett.* **2003**, *91*, 157405.
(30) Yan, J. A.; Yang, L.; Chou, M. Y. *Phys. Rev. B* **2007**, *76*, 115319.
(31) Becke, A. D. *J. Chem. Phys.* **1993**, *98*, 5648. Stephens, P. J.; Devlin, F. J.; Chabalowski, C. F.; Frisch, M. J. *J. Phys. Chem.* **1994**, *98*, 11623.
(32) Frisch, M. J.; Trucks, G. W.; Schlegel, H. B.; Scuseria, G. E.; Robb, M. A.; Cheeseman, J. R.; Montgomery, J. A., Jr.; Vreven, T.; Kudin, K. N.; Burant, J. C.; Millam, J. M.; Iyengar, S. S.; Tomasi, J.; Barone, V.; Mennucci, B.; Cossi, M.; Scalmani, G.; Rega, N.; Petersson, G. A.; Nakatsuji, H.; Hada, M.; Ehara, M.; Toyota, K.; Fukuda, R.; Hasegawa, J.; Ishida, M.; Nakajima, T.; Honda, Y.; Kitao, O.; Nakai, H.; Klene, M.; Li, X.; Knox, J. E.; Hratchian, H. P.; Cross, J. B.; Adamo, C.; Jaramillo, J.; Gomperts, R.; Stratmann, R. E.; Yazyev, O.; Austin, A. J.; Cammi, R.; Pomelli, C.; Ochterski, J. W.; Ayala, P. Y.; Morokuma, K.; Voth, G. A.; Salvador, P.; Dannenberg, J. J.; Zakrzewski, V. G.; Dapprich, S.; Daniels, A. D.; Strain, M. C.; Farkas, O.; Malick, D. K.; Rabuck, A. D.; Raghavachari, K.; Foresman, J. B.; Ortiz, J. V.; Cui, Q.; Baboul, A. G.; Clifford, S.; Cioslowski, J.; Stefanov, B. B.; Liu, G.; Liashenko, A.; Piskorz, P.; Komaromi, I.; Martin, R. L.; Fox, D. J.; Keith, T.; Al-Laham, M. A.; Peng, C. Y.; Nanayakkara, A.; Challacombe, M.; Gill, P. M. W.; Johnson, B.; Chen, W.; Wong, M. W.; Gonzalez, C.; Pople, J. A. *Gaussian 03, Revision C.02*; Gaussian, Inc.: Wallingford, CT, 2004.

NL900271Q